© 2023. Published by The Company of Biologists Ltd | Journal of Experimental Biology (2023) 226, jeb244692. doi:10.1242/jeb.244692

RESEARCH ARTICLE

A *cis*-regulatory sequence of the selector gene *vestigial* drives the evolution of wing scaling in *Drosophila* species

Keity J. Farfán-Pira[1], Teresa I. Martínez-Cuevas[1], Timothy A. Evans[2] and Marcos Nahmad[1,*]

ABSTRACT

Scaling between specific organs and overall body size has long fascinated biologists, being a primary mechanism by which organ shapes evolve. Yet, the genetic mechanisms that underlie the evolution of scaling relationships remain elusive. Here, we compared wing and fore tibia lengths (the latter as a proxy of body size) in *Drosophila melanogaster*, *Drosophila simulans*, *Drosophila ananassae* and *Drosophila virilis*, and show that the first three of these species have roughly a similar wing-to-tibia scaling behavior. In contrast, *D. virilis* exhibits much smaller wings relative to their body size compared with the other species and this is reflected in the intercept of the wing-to-tibia allometry. We then asked whether the evolution of this relationship could be explained by changes in a specific *cis*-regulatory region or enhancer that drives expression of the wing selector gene, *vestigial* (*vg*), whose function is broadly conserved in insects and contributes to wing size. To test this hypothesis directly, we used CRISPR/Cas9 to replace the DNA sequence of the predicted Quadrant Enhancer (vg^{QE}) from *D. virilis* for the corresponding vg^{QE} sequence in the genome of *D. melanogaster*. Strikingly, we discovered that *D. melanogaster* flies carrying the *D. virilis* vg^{QE} sequence have wings that are significantly smaller with respect to controls, partially shifting the intercept of the wing-to-tibia scaling relationship towards that observed in *D. virilis*. We conclude that a single *cis*-regulatory element in *D. virilis* contributes to constraining wing size in this species, supporting the hypothesis that scaling could evolve through genetic variations in *cis*-regulatory elements.

KEY WORDS: Allometry, Scaling, *Drosophila*, *Vestigial*, Quadrant Enhancer, CRISPR/Cas9

INTRODUCTION

Genetic and environmental factors contribute to morphological diversity across related species (Carroll, 2000). For instance, evolution of morphogenetic traits may be driven by environmental cues followed by selection of specific genetic variations in a population (Uller et al., 2018). The search for genetic variations that account for phenotypic changes across species has attracted the attention of evolutionary biologists for decades, but only recently have genome-editing technologies enabled us to test some predictions directly (Ryan and Farley, 2020). One way to study the genetic contributions to diversity in related species is to investigate how changes in the genome could explain the evolution of certain organs to whole-body scaling relationships (Evans, 2017; Van Belleghem et al., 2020).

To investigate scaling of a specific trait or body part, it is useful to evaluate quantitatively the relationship between the trait and the whole body (or representative trait) within the same individual. When body proportions do not change with body size, simple proportions may be used. Otherwise, scaling relationships should be used to analyze morphological changes that give rise to diversity and phenotypic variation in ecology and evolution (Esquerré et al., 2017; Galicia-Mendoza et al., 2021; Gomes Rodrigues et al., 2018; Shingleton, 2010). Depending on how scaling relationships are studied, allometries can be classified as ontogenic, when scaling relationships are studied during development and growth of an organism (Esquerré et al., 2017; Simons and Frost, 2021); static, when scaling relationships are studied within a population of individuals in a specific stage of development (Shingleton et al., 2008); and evolutionary, when scaling relationships are studied across different species (Tidière et al., 2017).

Mathematically, the scaling of any two traits or characters x and y within an organism can be modeled using the equation $y=bx^a$, where a and b are parameters that are fitted to data measurements of (x,y) pairs. When the value of $a=1$ cannot be ruled out statistically, we have a linear relationship in which the ratio y/x is a constant (given by b). However, when the null hypothesis of $a=1$ is rejected (i.e. the scaling relationship between x and y is not isometric), it is convenient to employ a logarithmic transformation to obtain a linear model of the allometric relationship:

$$\log(y) = a\log(x) + \log(b). \quad (1)$$

In Eqn 1, the transformed variables $\log(x)$ and $\log(y)$ are fitted to a linear transformation using standard linear-fitting procedures, where a is the slope of the line (also known as the allometric coefficient) and $\log(b)$ is the intercept (Gayon, 2000; Shingleton, 2010). Using this formalism, allometries have been used to understand how environmental conditions (such as temperature, nutrition and rearing density) influence natural variation and trigger variability in scaling patterns (Shingleton et al., 2009; Weber, 1990), and to investigate the relationships underlying morphological evolution across different species (Pélabon et al., 2014; Shingleton, 2010). However, the genetic mechanisms underlying the evolution of allometric relationships in a group of species are little understood.

One way to understand the genetic basis underlying the evolution and diversity of body traits is to investigate the influence of key genes (e.g. selector genes) on the allometric relationships (Eqn 1). Genetic changes that affect the sensitivity to environmental factors generally affect slopes or allometric coefficients (Emlen et al., 2012; Okada et al., 2019; Tang et al., 2011; Xu et al., 2015), but genetic modifications may also control the intercept of the scaling relationships, such as the wing–body versus haltere–body

[1]Department of Physiology, Biophysics and Neurosciences, Centre for Research and Advanced Studies of the National Polytechnic Institute (Cinvestav-IPN), Mexico City 07360, Mexico. [2]Department of Biological Sciences, University of Arkansas, Fayetteville, AR 72701, USA.

*Author for correspondence (mnahmad@fisio.cinvestav.mx)

K.J.F.-P., 0000-0002-5010-4241; T.I.M.-C., 0000-0002-0835-9953; T.A.E., 0000-0002-2756-8064; M.N., 0000-0001-6300-5608

Received 23 June 2022; Accepted 13 April 2023

Journal of Experimental Biology (2023) 226, jeb244692. doi:10.1242/jeb.244692

relationship in *Drosophila melanogaster* (Crickmore and Mann, 2006). Therefore, changes in the intercept of an organ to the whole-body scaling relationship across species may be attributed to the evolution of specific developmental genes or pathways, such as the regulation of selector genes (Fig. 1). In particular, the evolution of relative organ size may be studied by investigating genetic changes affecting regulatory networks that control the expression pattern of an organ-specific selector gene (Fig. 1A), the properties of the protein that is produced by the selector gene (e.g. stability, degradation or its ability to bind DNA or other proteins; Fig. 1B), or by modifications in *cis*-regulatory elements (promoters, enhancer or silencers) that drive its expression (Gracia-Latorre et al., 2022; Rebeiz and Tsiantis, 2017; Ryan and Farley, 2020) (Fig. 1C).

The *Drosophila* wing has been extensively used as a model system to understand the genetic basis of organ growth and morphogenesis (Gou et al., 2020; Neto-Silva et al., 2009; Tripathi and Irvine, 2022). In particular, it is a useful system to investigate quantitatively the variation of body traits under genetic and environmental manipulations. Adult wing size in *Drosophila* is determined by growth of a precursor organ, the wing imaginal disc, which is patterned and grows during larval development (Beira and Paro, 2016). Growth of the wing imaginal disc is driven by two morphogens: Wingless (Wg) emanating at the dorsal–ventral boundary, and Decantaplegic (Dpp), at the anterior–posterior boundary in the wing imaginal disc (Couso et al., 1995; Neumann and Cohen, 1996; Prasad et al., 2003). These morphogens act together with *vestigial* (*vg*), an evolutionarily conserved wing selector gene in holometabolous insects (Abouheif and Wray, 2002; Clark-Hachtel et al., 2013; Nel et al., 2013; Williams et al., 1991) in a regulatory network that triggers *vg* expression and wing growth through proliferation and cell recruitment (Muñoz-Nava et al., 2020; Parker and Struhl, 2020; Zecca and Struhl, 2007a,b). Through cell recruitment, Vg-expressing cells induce the propagation of the *vg* pattern via the Quadrant Enhancer (vg^{QE}) in a complex signal processing known as 'feed forward signal', which is fueled by Wg and Dpp signaling and implicates the polarization of the protocadherins Fat and Dachsous, that ultimately results in the nuclear translocation of the transcription factor Yorkie (Yki), where it finally activates transcription of *vg* (Muñoz-Nava et al., 2020; Neumann and Cohen, 1996; Parker and Struhl, 2020; Zecca and Struhl, 2007a,b, 2010).

Here, we investigated how wing sizes scale relative to tibia sizes (used as a proxy for whole-animal size) in four *Drosophila* species: *D. melanogaster*, *D. simulans*, *D. ananassae* and *D. virilis* (Fig. 2A). Although there are some significant deviations in the slopes of the static allometric relationships of these species, we immediately noticed that *D. virilis* has a dramatically different intercept than the other three species. This difference results from the fact that *D. virilis* individuals have a much smaller relative wing size compared with the other species. Thus, we asked whether the evolution of this scaling relationship is driven by changes in the *cis*-regulatory elements within the *vg* selector gene (Fig. 1C). To address this, we cloned the sequence of the predicted vg^{QE} in *D. virilis* and used the CRISPR/Cas9 system to replace these sequences into the *D. melanogaster* genome. Strikingly, in animals where the vg^{QE} of *D. melanogaster* was replaced by the corresponding vg^{QE} of *D. virilis*, wings exhibit a reduced relative wing size with respect to what would be expected in *D. melanogaster*. These results suggest that the vg^{QE} sequence plays an important role in the determination of size and the establishment of wing-to-body scaling relationships in *Drosophila* species.

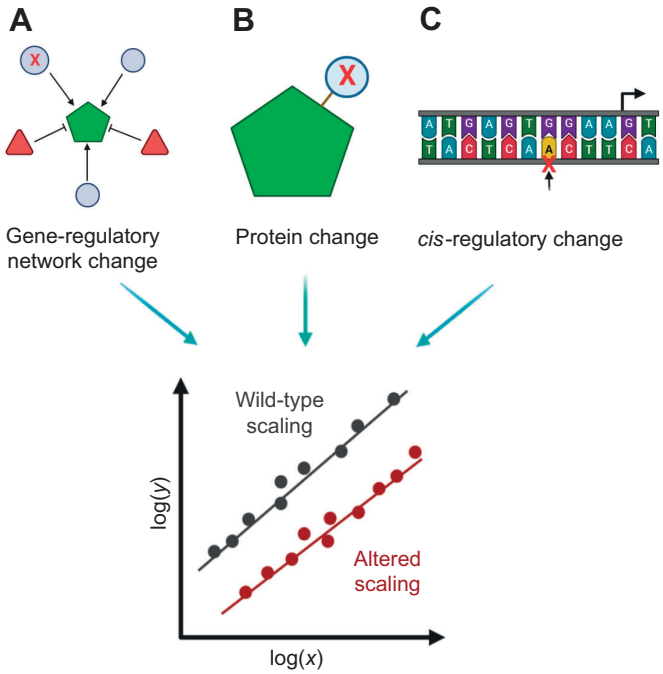

Fig. 1. Selector-gene mechanisms for the evolution of scaling relationships. Scaling relationships between two traits *x* and *y* may evolve by affecting (red 'X') a selector gene (represented by a green pentagon) in three different ways: (A) altering the expression or effect of an activator (light blue circle) or a repressor gene (red triangle); (B) affecting the stability, function or post-translational modification of the selector-gene protein product; or (C) causing a modification in the *cis*-regulatory region of the selector gene.

MATERIALS AND METHODS

Drosophila strains

The following *Drosophila* strains were used: *D. melanogaster* Meigen 1830 Samarkand strain (RRID:BDSC_4270, Bloomington Drosophila Stock Center); *y,w* strain of *D. melanogaster*, provided by Dr Fanis Missirlis (Cinvestav, Mexico); *D. simulans* Sturtevant 1919 (14021-0251.261, Drosophila Species Stock Center); *D. ananassae* Doleschall 1858 (14024-0371.00, Drosophila Species Stock Center); *D. virilis* Sturtevant 1916 (15010-1051.87, Drosophila Species Stock Center); w, ms1096-Gal4 (Bloomington Drosophila Stock Center RRID:BDSC_8860); UAS-vg^{RNAi} (Vienna Drosophila Resource Center 16896); nub-Gal4 (Bloomington Drosophila Stock Center RRID:BDSC_38418); *w; Sco/CyO, RFP* (available from Timothy A. Evans); *y,w*, nos-Cas9 (Bloomington Drosophila Stock Center RRID:BDSC_54591); and *D. melanogaster* (vg^{QEDmel}) and *D. melanogaster* (vg^{QEDvir}), both generated in this study. Adult flies were crossed and kept at 25°C in vials containing standard *Drosophila* food.

Scaling relationships

Adults were separated by sex (data in Figs 2 and 4 correspond to females, but equivalent results were obtained for males in Figs S2 and S4, respectively) using a stereoscopic microscope (Nikon SMZ800) and preserved in 1 ml of 70% ethanol for dehydration for at least 12 h for further analysis. Each specimen was dissected in 15 µl of ethanol 50% to obtain left/right wings, left/right fore legs and thorax, which were mounted in microscope slides using a stereoscopic microscope (Nikon SMZ800).

Wings, fore legs and thorax were photographed in a bright-field binocular microscope (Nikon Eclipse Ci) attached to a camera (ProgRes® CT5, Jenoptik) using the software ProgRes® Capture

Journal of Experimental Biology (2023) 226, jeb244692. doi:10.1242/jeb.244692

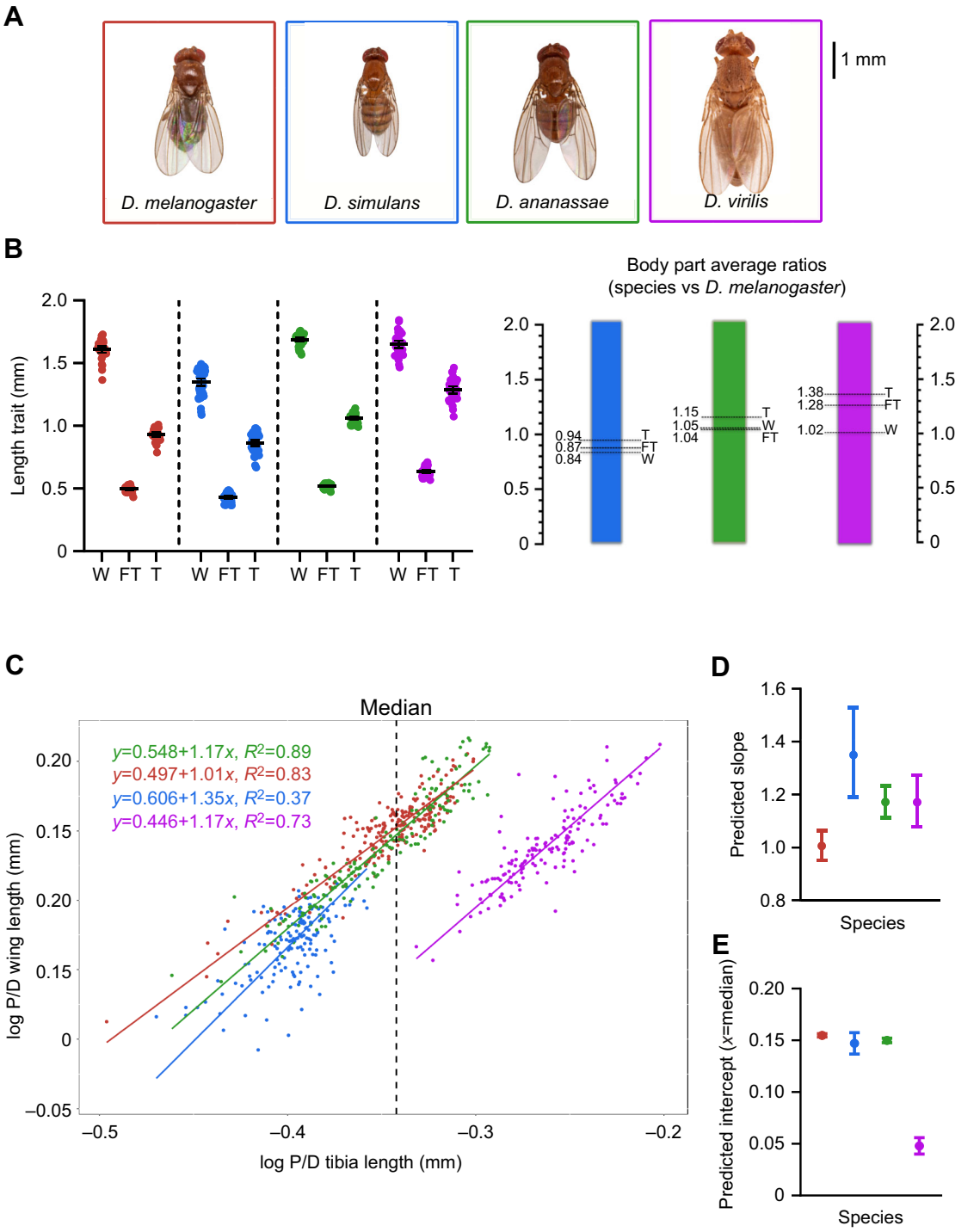

Fig. 2. Wing-to-tibia scaling relationships reveal a reduction of wing size in *Drosophila virilis* females. (A) Adults of *Drosophila* species used in this study. Square color indicates code color for subsequent figures. (B) Proximal–distal trait measures in *Drosophila* species. Average length of left/right wings (W) and fore tibias (FT), as well as thorax (T) measures are represented for each female fly. Right panel shows the body part average ratios (species versus *D. melanogaster*) for each measured trait (equivalent results were obtained for males; see Fig. S2). *D. melanogaster*, *n*=36; *D. simulans*, *n*=49; *D. ananassae*, *n*=35; *D. virilis*, *n*=35. (C) Wing-to-tibia static scaling relationships fitted using model II regression (SMA) in female *Drosophila* (see results obtained for males in Fig. S2). P/D, proximal/distal. (D) Predicted slope of wing–tibia scaling relationship for each *Drosophila* species. (E) Predicted intercept of wing–tibia scaling relationship for each *Drosophila* species. The predicted intercept value was obtained through SMA adjusted to the overall median log(tibia size) of all species (dashed line in C). Error bars are 95% confidence intervals. The experiment was replicated twice in the laboratory. *Drosophila melanogaster*, *n*=224; *D. simulans*, *n*=157; *D. ananassae*, *n*=169; *D. virilis*, *n*=156.

Pro-2.9. Measurements of proximal-distal length (P/D) (see Fig. S2A) were performed using ImageJ software (https://imagej.nih.gov/ij/download.html) (Schneider et al., 2012) after the corresponding calibration for the 4× objective (distance in pixels: 100.501; known distance: 0.1; pixel aspect ratio: 1.0, unit of length: mm). Each point in the allometry graphs corresponds to the average

Journal of Experimental Biology (2023) 226, jeb244692. doi:10.1242/jeb.244692

measurements of left/right wings and left/right fore legs of the same animal. We used standardized major axis (SMA) regression (Shingleton, 2019) to obtain the slope and intercepts for each population of flies.

Sequence alignment

Synteny of the *vg* gene in *D. melanogaster*, *D. simulans*, *D. ananassae* and *D. virilis* was evaluated through information from the NCBI (https://www.ncbi.nlm.nih.gov/) and OrthoDB databases (https://www.orthodb.org/). The search was limited to the fourth intron of the gene, and posteriorly paired/local alignments using the FASTA format through the Smith–Waterman algorithm (Smith and Waterman, 1981) in EMBOSS Water (Ubuntu 18.04; https://launchpad.net/ubuntu/bionic/+package/emboss) were developed (*D. melanogaster* QE versus *Drosophila* species introns): the length of each sequence was delimited based on the *D. melanogaster* reference sequence, followed by multiple alignments using Clustal Omega from EMBL-EBI (Madeira et al., 2022). The sequence of QE reported for *D. melanogaster* strain Samarkand (GenBank ID: FJ513071.1) was used as a template for searching corresponding QE sequences for *D. simulans*, *D. ananassae* and *D. virilis*. Alignment of representative QE regions in Fig. 3 and whole multiple sequence alignment was developed using BioEdit version 7.7.1 (see Fig. S5).

gRNA Design and construction of gRNA plasmids

Target sites were designed using the flyCRISPR online tool CRISPR Optimal Target Finder (https://flycrispr.org) (Gratz

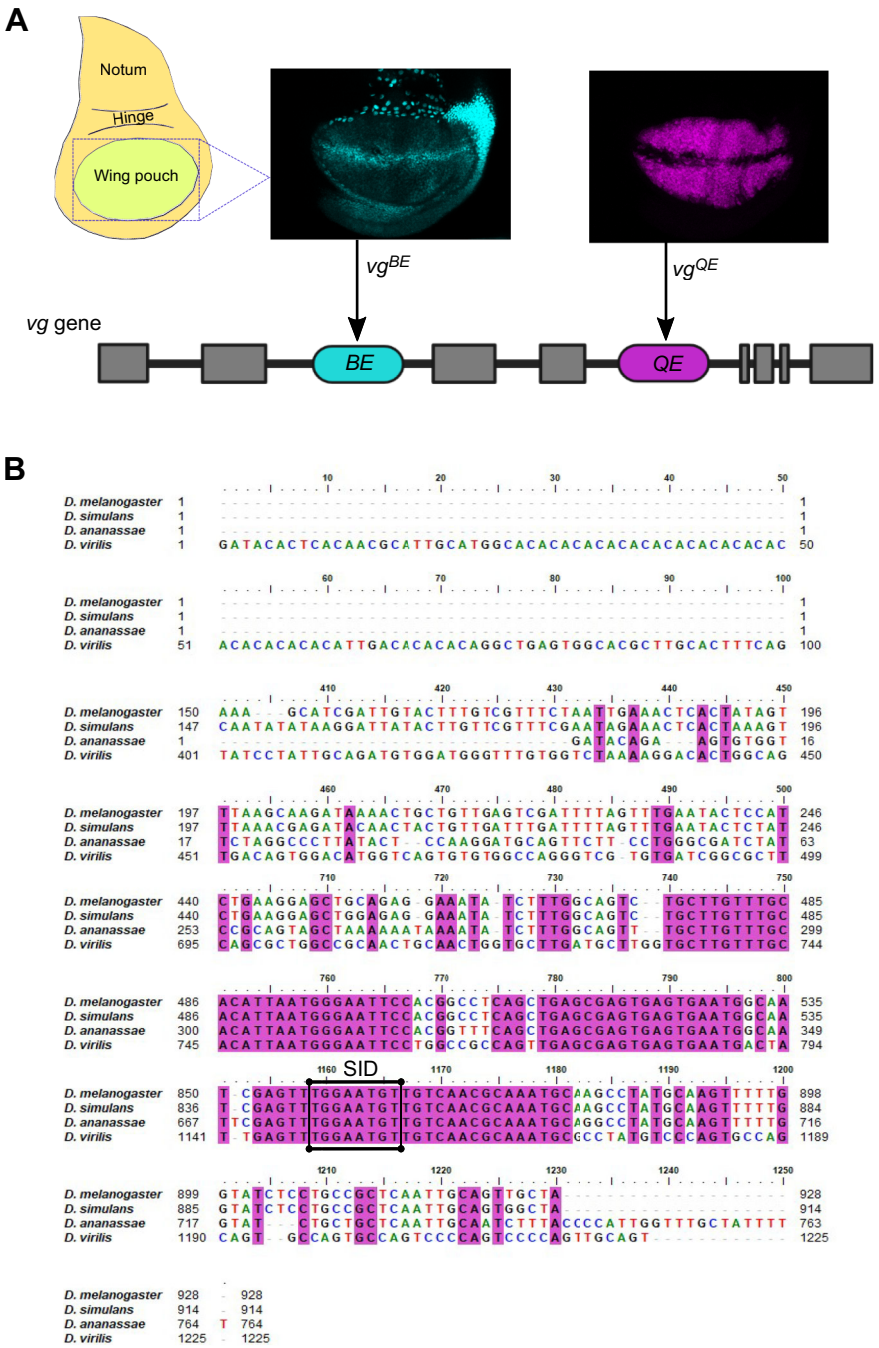

Fig. 3. Regulatory sequences of the *vg* gene in *Drosophila*. (A) Expression pattern of the *vg cis*-regulatory sequences in *D. melanogaster* (taken from Farfán-Pira et al., 2022). (B) Alignment of representative and conserved regions of vg^{QE} sequences in *Drosophila* species. Bases marked by a black square show conserved domains (Scalloped Interaction Domain, SID [TGGAATGT]) necessary for *vg* gene transcription.

Journal of Experimental Biology (2023) 226, jeb244692. doi:10.1242/jeb.244692

et al., 2014; Iseli et al., 2007). Cloning was performed into the pCFD4-U6:1_U6:3tandemgRNAs vector Addgene plasmid 49411, which allows tandem expression of two gRNA sequences (Evans, 2017; Port et al., 2014), through PCR amplification using pair of primers 2 and 3 (Table S1) with a 2X Phusion Flash PCR Master Mix (Thermo Fisher Scientific, catalog no. F548S). Gibson Assembly (New England Biolabs, catalog no. E2611) was performed with PCR products and pCFD4 *Bbs*I (New England Biolabs, catalog no. R0539L) digested vector. All cloning products were confirmed by DNA sequencing before injection.

Construction of QE donor plasmids

The donor plasmid was assembled using overlap extension PCR (Heckman and Pease, 2007). We first designed a working base vector composed of four PCR fragments: two that were derived from plasmid backbone of pHD-DsRed (Addgene plasmid 51434; https://www.addgene.org/51434/) (primer pair 835, 836), DsRed fluorescent coding region (primer pair 837, 838), and two derived from genomic DNA of *D. melanogaster*, left homologous arm (LHA2) (primer pair 839, 840) and right homologous arm (RHA1) (primer pair 841, 842). We then assembled the LHA2-DsRed-RHA1 fragments in one round of PCR (primer pair 839, 842) and then

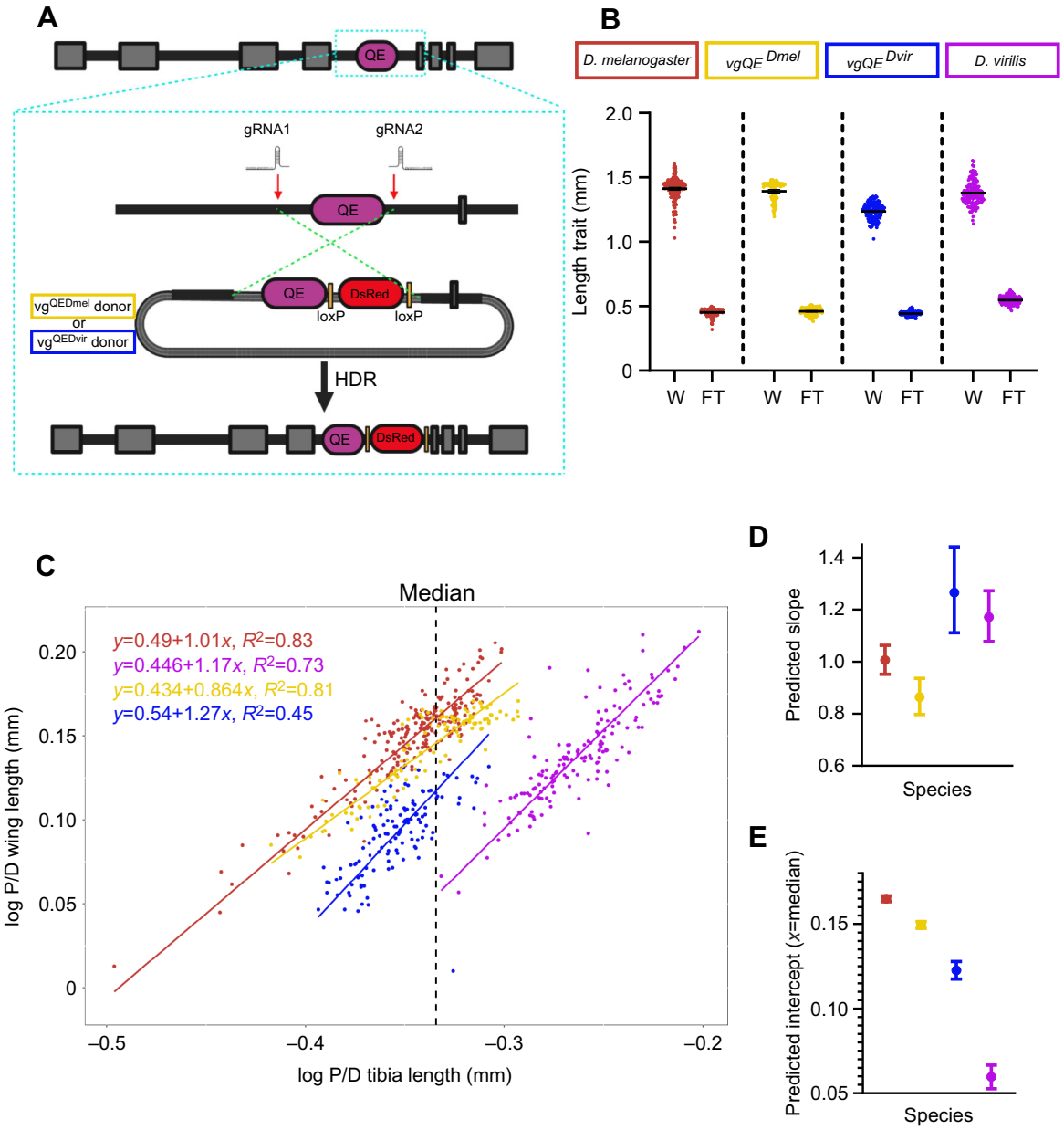

Fig. 4. *Drosophila virilis* vg^{QE} replacement into *D. melanogaster* results in allometric changes. (A) *vg* gene, QE (magenta box) and target region for replacement with CRISPR/cas9 Homologous Directed Repair (HDR) system is delimited by gRNAs 1 and 2, and the donor plasmid constructions with QE sequences for each species are represented. (B) Color code and proximal–distal trait measures in *Drosophila* species (*D. melanogaster*, *D. virilis*) and CRISPR/Cas9 mutants (vg^{QEDmel}, vg^{QEDvir}). Average length of left/right wings and fore tibias are represented for each female flies. (C) Wing-to-tibia static relationships fitted using model II regression (SMA). (D) Predicted slope of wing–tibia scaling relationship for *D. melanogaster*, *D. virilis* and CRISPR/Cas9 stocks. (E) Predicted intercept of wing–tibia scaling relationship for *D. melanogaster*, *D. virilis* and CRISPR/Cas9-edited stocks. The predicted intercept value was obtained through SMA adjusted to the overall median log(tibia size) of *D. melanogaster*, *D. virilis* and CRISPR/Cas9 stocks (dashed line in C). Error bars are 95% confidence intervals. *D. melanogaster*, n=224; vg^{QEDmel}, n=120; vg^{QEDvir}, n=128; *D. virilis*, n=156.

combined this product with the plasmid backbone fragment in a second PCR to obtain the whole base vector as a linear fragment: pHD-DsRed-LHA2-DsRed-RHA1 (primer pair 837, 843). The PCR product was transformed directly into competent *E. coli* and circularized *in vivo* (Watson and García-Nafría, 2019). To insert the specific QE sequences, we amplified by PCR the sequences from genomic preparations of *D. melanogaster* (primer pair 844, 845) and *D. virilis* (primer pair 844, 846) and assembled with the base vector through overlap extension PCR. All the components of the donor vector, including the QE, were sequenced prior to injection.

Identification of CRISPR-modified alleles

The vg^{QE} gRNA plasmid was co-injected with the QE homologous donor plasmids into nos-Cas9 embryos using the service provided by Rainbow Transgenic Flies (Camarillo, CA, USA). Individuals recovered from injected embryos were crossed to *w*; *Sco/CyoRFP* flies. *CyORFP* or *Sco* flies from this cross (potentially carrying vg^{QE} HDR alleles) were screened for red fluorescent eyes (indicating genomic integration of DsRed sequences carried on the HDR donor plasmid; see Fig. S3). Fluorescent-eye flies were then crossed back individually to *w*; *Sco/CyORFP* to generate balanced stocks. Confirmation of the inserted sequences was tested by PCR using primers 20, 23, 41, 44, 47 and 53 (Table S1, Fig. S3). PCR-confirmed balanced stocks with the modified alleles were also confirmed through genomic DNA sequencing.

Statistical analysis

Scaling relationship data were analyzed using R version 4.1.2 (https://www.r-project.org/) and RStudio (https://www.rstudio.com/) version 4.1.2. The collected data were analyzed using an SMA model II regression (Shingleton, 2019; Warton et al., 2006; Wilcox et al., 2022 preprint) and computed 95% confidence intervals through the SMATR package in R (Warton et al., 2012; script is available in GitHub). Wing and tibia lengths were analyzed using GraphPad Prism 8.0.1 Software (https://www.graphpad.com/scientific-software/prism/). For pairwise statistical comparisons, Student's *t*-tests were used with $P<0.05$ to define significance.

RESULTS

Wings of *D. virilis* have reduced relative wing size compared with the other *Drosophila* species

Although several measures of whole-body size (e.g. mass or pupal case) have been used in *Drosophila* studies (Mirth and Shingleton, 2012; Morin et al., 1996; Stillwell et al., 2011), we looked for a trait that could serve as a reference to draw allometric relationships with the wings. The length of the tibia in legs has been used as a proxy for body size measures in several dipterans (Krause et al., 2019; Reigada and Godoy, 2005; Rohner et al., 2018; Tran et al., 2020), and is considered a standard for body size in other insects, such as parasitoid wasps (Sagarra et al., 2001; Thorne et al., 2006). Tibias can be much more reliably measured and directly compared with the proximal–distal (PD) length of the adult wing than other whole-body measures such as the thorax (Fig. 2B; see Materials and Methods). In addition, legs are not affected by changes in *vg* expression (Fig. S1A,B). To further justify the use of tibias as a proxy of body size, we compared the wings, fore tibias and thorax of individuals in each of the four species shown in Fig. 2A (*D. melanogaster*, *D. simulans*, *D. ananassae* and *D. virilis*; Fig. 2B). Using mean trait measurements in each species (e.g. $\text{mean\_thorax}_{\text{Species}}$), we can compute wing, fore tibia and thorax ratios of each species relative to *D. melanogaster* (e.g. $\text{mean\_thorax}_{\text{Species}}/\text{mean\_thorax}_{\text{Dmel}}$). The thorax ratio (T) reveals that *D. simulans* is smaller than *D. melanogaster* (T<1, blue bar of Fig. 2B and Fig. S2A) and *D. ananassae* is slightly larger (T>1, green bar in Fig. 2B and Fig. S2A), but *D. virilis* is much larger (T>>1, magenta bar in Fig. 2B and Fig. S2A; see also LaRue et al., 2015; Schoofs et al., 2010). Fore tibia ratios (FT) follow similar (although not the same) relationships relative to *D. melanogaster* (see green bars Fig. 2B and Fig. S2A), suggesting that fore tibias (for simplicity referred as tibias thereafter) can be used as a proxy for body size. However, the wing ratio (W) in *D. virilis* remains almost unchanged relative to *D. melanogaster* (W=1.02, females and W=1.1, males; magenta bar in Fig. 2B and Fig. S2A). We then proceeded to obtain the population scaling relationships (static allometry) between wings and tibias of each species using the SMA model II regression (see Materials and Methods; Table 1, Fig. 2C; Fig. S2B).

To make a comparison across species, we computed the 95% confidence intervals of the slope and intercept of each scaling relationship (Fig. 2D,E). Notably, the slope of *D. melanogaster* exhibits an isometric behavior (slope of 1 contained in the 95% confidence interval), but *D. simulans*, *D. ananassae* and *D. virilis* all exhibit slopes larger than 1 (Table 1). Although this slope effect is interesting on its own (see Discussion), we decided to focus our attention on a more dramatic result, namely, the difference in intercept between *D. virilis* and the rest of the species (Fig. 2C,E). Because the intercept is arbitrarily computed at 0, which is far away from the average tibia size, we computed the intercept of the scaling relationships at the median value of the tibia for all the data (dashed line in Fig. 2C and Fig. S2B). Remarkably, the 95% confidence intervals of the intercepts at the median show a dramatic difference in relative wing size.

Bioinformatic identification of regulatory elements within the vg^{QE} sequence

We considered the possibility that the difference in the intercept of these wing-to-tibia scaling relationships was controlled by *cis*-regulatory elements of the *vg* gene (Fig. 1C). From the two intronic *cis*-regulatory elements that drive *vg* expression (Fig. 3), we focused on the vg^{QE} because it controls expression in most of the wing pouch (compare cyan and magenta patterns in Fig. 3A), and previous work has implicated this element in wing growth (Muñoz-Nava et al., 2020; Parker and Struhl, 2020; Zecca and Struhl, 2007b). We first examined the sequence of the reported vg^{QE} (Dworkin et al., 2009; GenBank ID: FJ513071.1), in order to determine whether a *cis*-regulatory element also exists in the other three *Drosophila* species. We then aligned the sequences of the whole fourth intron of each four species selected. The alignment recovers sequence conservation and the presence of regulatory domains to promote *vg* transcription (as the

Table 1. Slopes and intercepts of wing–tibia static scaling relationships in females (F) and males (M) of different *Drosophila* species

Species	Sex	Slope	Intercept
D. melanogaster	F	1.005 [0.951,1.063]	0.496 [0.477,0.516]
	M	0.805 [0.740,0.876]	0.388 [0.363,0.413]
D. simulans	F	1.349 [1.190,1.529]	0.605 [0.538,0.673]
	M	1.117 [0.976,1.280]	0.483 [0.421,0.546]
D. ananassae	F	1.171 [1.112,1.233]	0.548 [0.526,0.569]
	M	1.095 [1.038,1.155]	0.475 [0.454,0.496]
D. virilis	F	1.171 [1.077,1.272]	0.446 [0.420,0.471]
	M	1.344 [1.258,1.436]	0.482 [0.458,0.507]

Slopes, intercept values and 95% confidence intervals (shown in brackets). α=0.05. Model II of SMA regression was used to fit the line.

Journal of Experimental Biology (2023) 226, jeb244692. doi:10.1242/jeb.244692

Scalloped Interaction Domain, SID), an aspect that allowed us to predict a vg^{QE} in each of these species (Fig. 3B).

CRISPR/Cas9-HDR replacement of the vg^{QE} from *D. virilis* into the *D. melanogaster* genome

To evaluate the influence of the vg^{QE} in *Drosophila* wing allometry, we use the CRISPR/Cas9 Homologous Directed Repair (HDR) system (Evans, 2017; Port et al., 2014) to replace the vg^{QE} sequence in *D. melanogaster* with the predicted vg^{QE} from other species. We decided to replace only with the vg^{QE} of *D. virilis* because it was the only species in which we obtained a dramatic change in wing-to-tibia allometries (Fig. 2C and Fig. S2B). Thus, we designed a guide RNA (gRNA) expression vector using a pCFD4 backbone (Howard et al., 2021; Port et al., 2014) that contains two gRNA sequences to target the vg^{QE} region in *D. melanogaster* (Fig. 4A). We then generated a vg^{QE} homologous donor plasmid containing the sequence of the predicted vg^{QE} of *D. virilis* and *D. melanogaster* (as a control) to act as a template for the HDR repair system (Fig. 4A). The experimental design of this donor construct allowed us to generate a base vector, which contains left and right *D. melanogaster* homologous arms and DsRed, that could work as a single vector to produce different vg^{QE} replacements using the same gRNA sequences and donor backbone of pHD-DsRed (Fig. 4A). Plasmids with the gRNAs and the *D. virilis* or *D. melanogaster* vg^{QE} vectors were verified through PCR (Fig. S3) and injected into embryos that maternally carry the Cas9 endonuclease (nos-Cas9 flies) to generate the vg^{QE}-replaced flies.

Replacement of the vg^{QE} from *D. virilis* into the *D. melanogaster* genome reduces relative wing size

After obtaining stable stocks in which the vg^{QE} of *D. melanogaster* (vg^{QEDmel}) or *D. virilis* (vg^{QEDvir}) was replaced with the endogenous vg^{QE} of *D. melanogaster*, we asked whether these replacements could affect the wing-to-tibia scaling relationships. With this aim, we generated homozygous stocks (except in the case of vg^{QEDmel}, for which homozygous animals were not viable and we used vg^{QEDmel}/+ flies instead) and plotted length traits (Fig. 4B; Fig. S4A) and static scaling relationships as we did for wild-type animals, using the model II regression (SMA) (Fig. 4C–E and Fig. S4B–D). Tibia measurements are only slightly (although significantly) different in vg^{QEDmel} and vg^{QEDvir} flies (Fig. 4B; Fig. S4A), but vg^{QEDvir} animals have a marked relative reduction in wing length with respect to vg^{QEDmel} controls and wild-type *D. melanogaster* itself (Fig. 4B; Fig. S4A). This suggests that the vg^{QE} of *D. virilis* likely carries genetic information to reduce relative wing size. However, this effect was not as dramatic as in wild-type *D. virilis*, as revealed by the wing-to-tibia scaling relationships (Fig. 4C; Fig. S4B), suggesting that other inputs are needed to achieve the degree of relative wing size reduction that *D. virilis* exhibits.

Following the analysis that we performed in wild-type flies, we computed the 95% confidence intervals of slopes and intercepts in the CRISPR-replaced stocks (Fig. 4D,E). Our analysis shows that vg^{QEDvir} animals have a marked reduction in wing length with respect to vg^{QEDmel} controls, although they do not exhibit the same effect in the intercept as in wild-type *D. virilis* flies. Nonetheless, this experiment reveals that a single *cis*-regulatory element has the potential to modulate scaling relationships in animals.

DISCUSSION

The evolution of scaling relationships between body parts is a major source of phenotypic diversity in animals. The diversity of wing to whole-body relationships among insect species displays an astonishing repertoire of allometries; butterflies have enormous wings compared with their bodies, while bees have quite the opposite wing-to-body ratio. While the evolution of these scaling relationships is likely to be very complex among distant species, the evolution of wing to whole-body scaling in more closely related species may be pinpointed to the evolution of specific regulatory changes in the genome. The *cis*-regulatory hypothesis, in which phenotypes evolve through changes in *cis*-regulatory regions of key genes has received a lot of attention in the literature (Carroll et al., 2005; Jiggins et al., 2017; Rebeiz and Tsiantis, 2017; Wray, 2003, 2007); however, very few examples in which evolutionary changes have been mapped to specific *cis*-regulatory interactions have been reported (Stern and Orgogozo, 2009; Wittkopp and Kalay, 2011).

In this work, we used CRISPR-mediated replacement (Fig. 4A) of a specific regulatory sequence within the *vg* wing selector gene from *D. virilis*, which diverged from *D. melanogaster* at least 40 million years ago (Powell and DeSalle, 1995) and displays a reduction of wings relative to the rest of the body (Figs 2 and 4), into the genome of *D. melanogaster*. We found that this *cis*-regulatory element itself does contribute, at least partially, to a change in the intercept of the allometric relationship (Fig. 4C; Fig. S4B), providing support for the hypothesis that evolution of scaling relationships could be driven by genetic variations in the vg^{QE} sequence. It is unclear, however, whether the common ancestor of these species had a relative wing size such as in species of the *melanogaster* group or a smaller relative wing size such as in *D. virilis*, but our data support that an important evolutionary event at the vg^{QE} took place after the split of these groups (Fig. 5).

Although we do not focus on changes in slopes in this study, we reported statistically significant differences in the slopes of allometric relationships (Table 1 and Fig. 2C). The elucidation of slopes in wing-to-tibia scaling relationships of these and other *Drosophila* species might shed light on how traits generate the characteristic diversity of individual species (Wilcox et al., 2023). However, future studies examining slope changes of specific

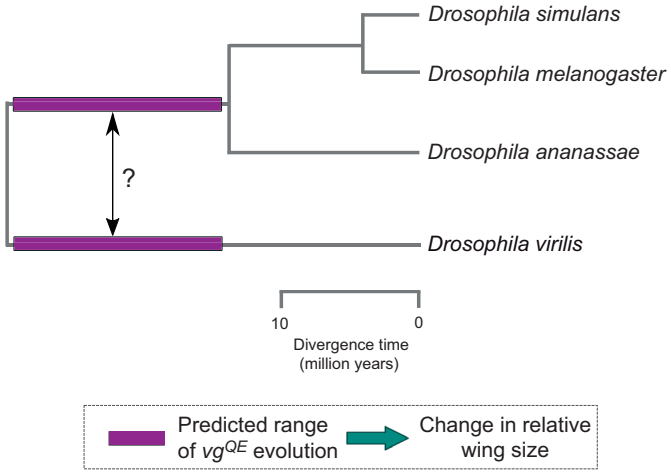

Fig. 5. Changes in the vg^{QE} that regulate relative wing size took place at the split between the *melanogaster* and *virilis* groups. The evolutionary event (purple rectangles) that generated different relative wing sizes in these *Drosophila* species likely took place after the split between the *melanogaster* and *virilis* groups, at least 40 million years ago. The regulatory change took place either in the ancestor lineage of the *melanogaster* group, favoring larger wings relative to body size in *D. melanogaster*, *D. simulans* and *D. ananassae*; or in the ancestor lineage of the *virilis* group, favoring smaller wings relative to body size in *D. virilis*.

species in response to environmental effects such as temperature or nutrition may reveal how differences in relative wing sizes among species evolved (Shingleton et al., 2009).

How could the replacement of a *cis*-regulatory element affect the ability to scale the size of an organ with respect to the size of another reference within the animal? Under the experimental conditions evaluated, the vg^{QEDvir} may adjust its response to Dpp and Wg, morphogens that have been shown to directly affect wing development in *D. melanogaster* (Parker and Struhl, 2020). The reduced growth of wings in vg^{QEDvir} mutants could be a result of changes in morphogen spread or degradation in the common ancestor of *D. virilis* and *D. melanogaster*. In this context, mathematical modeling approaches underlying the dynamics of morphogen gradients that govern wing development could serve as hypothesis-generation tools to determine the possible evolutionary trajectories driving the observed wing diversity in these *Drosophila* species.

Another approach for inferring possible molecular mechanisms that could explain the observed changes in relative wing size is through bioinformatic analysis. For instance, in addition to the participation of Wg and Dpp in QE activation and *vg* autoregulation (Parker and Struhl, 2020; Zecca and Struhl, 2007a), a previous study in *D. melanogaster* and *D. virilis* suggest that Dpp has a positive role and Wg has a negative role in the regulation of an enhancer that promotes visceral mesoderm induction (Lee and Frasch, 2005). A DFR (*Drosophila* Drifter) POU Domain transcription factor has also been described in *D. virilis* and *D. melanogaster* that binds to an adjacent site in QE MAD-binding site that may be essential to QE activation in the wing pouch, through a complex between MAD and DFR (Certel et al., 2000). This MAD site is apparently also a binding site for Brinker (Brk), presumably acting as a competing repressor of *vg* transcription (Kirkpatrick et al., 2001). Perhaps in the vg^{QEDvir} flies, Brk-mediated repression is somehow favored, altering morphogen spreading and the relative size of the wing. This vg^{QEDvir} repressor hypothesis could also explain why when we delete the vg^{QE} sequence in *D. melanogaster*, the wing phenotype is fully rescued (Farfán-Pira et al., 2022), presumably through the action of shadow enhancers (Hong et al., 2008), but in the vg^{QEDvir} replacement the wing phenotype is not.

The vg^{QE} sequence has also been studied to determine which components are necessary to induce *vg* transcription, where SID domains of Scalloped (Sd) interact with DNA consensus sequence (TGGAATGT) located in the QE region (Halder et al., 1998; Klein and Arias, 1999; Simmonds et al., 1998). As we noted in our alignment (Fig. 3B and Fig. S5), SID domains are evolutionarily conserved in the four species examined, suggesting that this role of Sd to form a complex with Vg is a conserved mechanism to induce the transcriptional mechanism of *vg* expression in *Drosophila*. However, additional sites within the QE also influence *vg* transcription; for example, the *Drosophila* transcription factor Mothers Against Dpp (MAD) has an N-terminal homology region (mad1) that binds within the QE (GCCGnCGC) sequence in *D. melanogaster* and has a role in direct expression of *vg* in the pouch and wing formation. Furthermore, mutation of this consensus sequence and the inhibition of interaction between MAD and the QE sequence produces animals with smaller wings (Certel et al., 2000; Kim et al., 1997). According to a previous report, in *D. virilis*, the MAD binding site is present in the sequence of regulatory sequences of the *daughters against dpp* (*dad*) gene (Weiss et al., 2010), suggesting that *D. virilis* may have similar mechanisms of *vg* regulation by MAD in QE sequences, but further examination is necessary to confirm or refute this hypothesis.

Strikingly, the presence of vg^{QE} sequences located in the fourth intron of the *vg* gene in the honey bee *Apis mellifera* (which diverged from *Drosophila* about 300 million years ago) shows similar patterns of expression in imaginal wing discs (Prasad et al., 2016). Thus, the evolutionary conservation of QE in other insect groups suggests that the *cis*-regulatory role of the vg^{QE} in driving wing scaling relationships may be relevant in more distant species as well.

Acknowledgements
We thank José Luis Fernández-López and Rafael Rodríguez-Muñoz for technical assistance. We are grateful to the core facilities at Cinvestav-IPN and the University of Arkansas for providing us access to equipment to conduct the experiments for this study. We thank Eduardo Ochoa for taking and sharing the photos of the specimens in Fig. 2. We also thank Ehab Abouheif, Fanis Missirlis, Augusto Cesar Poot-Hernández and members of the Nahmad and Evans laboratories for discussions.

Competing interests
The authors declare no competing or financial interests.

Author contributions
Conceptualization: T.A.E., M.N.; Methodology: K.J.F.-P., T.I.M.-C., T.A.E., M.N.; Formal analysis: K.J.F.-P., T.I.M.-C., T.A.E., M.N.; Resources: T.A.E.; Data curation: K.J.F.-P., T.I.M.-C.; Writing - original draft: K.J.F.-P., M.N.; Writing - review & editing: K.J.F.-P., T.I.M.-C., T.A.E., M.N.; Visualization: K.J.F.-P., T.I.M.-C., M.N.; Supervision: T.A.E., M.N.; Funding acquisition: T.A.E., M.N.

Funding
This work was supported by the Consejo Nacional de Ciencia y Tecnología of México (CONACyT), grant number CB-2014-01-236685 to M.N. and PhD fellowship (487729) awarded to K.J.F.-P., and the National Institutes of Health (NIH) grant number R15 NS-098406 to T.A.E. We thank The Company of Biologists for a Travelling Fellowship grant DEVTF2105555 (https://www.biologists.com/travelling-fellowships/) awarded to K.J.F.-P. Deposited in PMC for release after 12 months.

Data availability
Data are available from GitHub (https://github.com/KeiFarfan/evo-devoDrosophila.git).

ECR Spotlight
This article has an associated ECR Spotlight interview with Keity Farfán-Pira.

References
Abouheif, E. and Wray, G. A. (2002). Evolution of the gene network underlying wing polyphenism in ants. *Science* **297**, 249-252. doi:10.1126/science.1071468

Beira, J. V. and Paro, R. (2016). The legacy of *Drosophila* imaginal discs. *Chromosoma* **125**, 573-592. doi:10.1007/s00412-016-0595-4

Carroll, S. B. (2000). Endless forms: the evolution of gene regulation and morphological diversity. *Cell* **101**, 577-580. doi:10.1016/S0092-8674(00)80868-5

Carroll, S. B., Grenier, J. K. and Weatherbee, S. (2005). *From DNA to Diversity: Molecular Genetic and the Evolution of Animal Design*, 2nd edn. Blackwell Publishing.

Certel, K., Hudson, A., Carroll, S. B. and Johnson, W. A. (2000). Restricted patterning of vestigial expression in *Drosophila* wing imaginal discs requires synergistic activation by both Mad and the drifter POU domain transcription factor. *Development* **127**, 3173-3183. doi:10.1242/dev.127.14.3173

Clark-Hachtel, C. M., Linz, D. M. and Tomoyasu, Y. (2013). Insights into insect wing origin provided by functional analysis of vestigial in the red flour beetle, *Tribolium castaneum*. *Proc. Natl. Acad. Sci. USA* **110**, 16951-16956. doi:10.1073/pnas.1304332110

Couso, J. P., Knust, E. and Martinez Arias, A. (1995). Serrate and wingless cooperate to induce vestigial gene expression and wing formation in *Drosophila*. *Curr. Biol* **5**, 1437-1448. doi:10.1016/S0960-9822(95)00281-8

Crickmore, M. A. and Mann, R. S. (2006). Hox control of organ size by regulation of morphogen production and mobility. *Science* **313**, 63-68. doi:10.1126/science.1128650

Dworkin, I., Kennerly, E., Tack, D., Hutchinson, J., Brown, J., Mahaffey, J. and Gibson, G. (2009). Genomic consequences of background effects on scalloped mutant expressivity in the wing of *Drosophila melanogaster*. *Genetics* **181**, 1065-1076. doi:10.1534/genetics.108.096453

Emlen, D. J., Warren, I. A., Johns, A., Dworkin, I. and Lavine, L. C. (2012). A mechanism of extreme growth and reliable signaling in sexually selected ornaments and weapons. *Science* **337**, 860-864. doi:10.1126/science.1224286

Esquerré, D., Sherratt, E. and Keogh, J. S. (2017). Evolution of extreme ontogenetic allometric diversity and heterochrony in pythons, a clade of giant and dwarf snakes. *Evolution* **71**, 2829-2844. doi:10.1111/evo.13382
Evans, T. A. (2017). CRISPR-based gene replacement reveals evolutionarily conserved axon guidance functions of *Drosophila* Robo3 and *Tribolium* Robo2/3. *Evodevo* **8**, 10. doi:10.1186/s13227-017-0073-y
Farfán-Pira, K. J., Martínez-Cuevas, T. I., Reyes, R., Evans, T. A. and Nahmad, M. (2022). The *vestigial* Quadrant Enhancer is dispensable for pattern formation and development of the *Drosophila* wing. *microPublication Biol*. doi:10.17912/micropub.biology.000585
Galicia-Mendoza, D. I., Sanmartín-Villar, I., García-Miranda, Ó. and Cordero-Rivera, A. (2021). Territorial damselflies are larger and show negative allometry in their genitalia. *Biol. J. Linn. Soc* **134**, 697-706. doi:10.1093/biolinnean/blab109
Gayon, J. (2000). History of the concept of allometry. *Am. Zool* **40**, 748-758.
Gomes Rodrigues, H., Cornette, R., Clavel, J., Cassini, G., Bhullar, B.-A. S., Fernández-Monescillo, M., Moreno, K., Herrel, A. and Billet, G. (2018). Differential influences of allometry, phylogeny and environment on the rostral shape diversity of extinct South American notoungulates. *R. Soc. Open Sci.* **5**, 171816. doi:10.1098/rsos.171816
Gou, J., Stotsky, J. A. and Othmer, H. G. (2020). Growth control in the *Drosophila* wing disk. *Wiley Interdiscip. Rev. Syst. Biol. Med* **12**, e1478.
Gracia-Latorre, E., Pérez, L., Muzzopappa, M. and Milán, M. (2022). A single WNT enhancer drives specification and regeneration of the Drosophila wing. *Nat. Commun.* **13**, 4794. doi:10.1038/s41467-022-32400-2.
Gratz, S. J., Ukken, F. P., Rubinstein, C. D., Thiede, G., Donohue, L. K., Cummings, A. M. and O'Connor-Giles, K. M. (2014). Highly specific and efficient CRISPR/Cas9-catalyzed homology-directed repair in *Drosophila*. *Genetics* **196**, 961-971. doi:10.1534/genetics.113.160713
Halder, G., Polaczyk, P., Kraus, M. E., Hudson, A., Kim, J., Laughon, A. and Carroll, S. (1998). The Vestigial and Scalloped proteins act together to directly regulate wing-specific gene expression in *Drosophila*. *Genes Dev.* **12**, 3900-3909. doi:10.1101/gad.12.24.3900
Heckman, K. L. and Pease, L. R. (2007). Gene splicing and mutagenesis by PCR-driven overlap extension. *Nat. Protoc* **2**, 924-932. doi:10.1038/nprot.2007.132
Hong, J.-W., Hendrix, D. A. and Levine, M. S. (2008). Shadow enhancers as a source of evolutionary novelty. *Science* **321**, 1314. doi:10.1126/science.1160631
Howard, L. J., Reichert, M. C. and Evans, T. A. (2021). The Slit-binding Ig1 domain is required for multiple axon guidance activities of *Drosophila* Robo2. *Genesis* **59**, e23443. doi:10.1002/dvg.23443
Iseli, C., Ambrosini, G., Bucher, P. and Jongeneel, C. V. (2007). Indexing strategies for rapid searches of short words in genome sequences. *PLoS One* **2**, e579. doi:10.1371/journal.pone.0000579
Jiggins, C. D., Wallbank, R. W. R. and Hanly, J. J. (2017). Waiting in the wings: what can we learn about gene co-option from the diversification of butterfly wing patterns? *Philos. Trans. R. Soc. Lond. B. Biol. Sci* **372**, 20150485. doi:10.1098/rstb.2015.0485
Kim, J., Johnson, K., Chen, H. J., Carroll, S. and Laughon, A. (1997). Drosophila Mad binds to DNA and directly mediates activation of vestigial by Decapentaplegic. *Nature* **388**, 304-308. doi:10.1038/40906
Kirkpatrick, H., Johnson, K. and Laughon, A. (2001). Repression of dpp targets by binding of brinker to mad sites. *J. Biol. Chem* **276**, 18216-18222. doi:10.1074/jbc.M101365200
Klein, T. and Arias, A. M. (1999). The vestigial gene product provides a molecular context for the interpretation of signals during the development of the wing in *Drosophila*. *Development* **126**, 913-925. doi:10.1242/dev.126.5.913
Krause, T., Spindler, L., Poeck, B. and Strauss, R. (2019). *Drosophila* acquires a long-lasting body-size memory from visual feedback. *Curr. Biol* **29**, 1833-1841.e3. doi:10.1016/j.cub.2019.04.037
LaRue, K. M., Clemens, J., Berman, G. J. and Murthy, M. (2015). Acoustic duetting in *Drosophila virilis* relies on the integration of auditory and tactile signals. *Elife* **4**, e07277. doi:10.7554/eLife.07277
Lee, H.-H. and Frasch, M. (2005). Nuclear integration of positive Dpp signals, antagonistic Wg inputs and mesodermal competence factors during *Drosophila* visceral mesoderm induction. *Development* **132**, 1429-1442. doi:10.1242/dev.01687
Madeira, F., Pearce, M., Tivey, A. R. N., Basutkar, P., Lee, J., Edbali, O., Madhusoodanan, N., Kolesnikov, A. and Lopez, R. (2022). Search and sequence analysis tools services from EMBL-EBI in 2022. *Nucleic Acids Res*. **50**, W276-W279. doi:10.1093/nar/gkac240
Mirth, C. K. and Shingleton, A. W. (2012). Integrating body and organ size in *Drosophila*: recent advances and outstanding problems. *Front. Endocrinol.* **3**, 49. doi:10.3389/fendo.2012.00049
Morin, J., Moreteau, B., Pétavy, G., Imasheva, A. and David, J. (1996). Body size and developmental temperature in *Drosophila simulans*: comparison of reaction norms with sympatric *Drosophila melanogaster*. *Genet. Sel. Evol* **28**, 415. doi:10.1186/1297-9686-28-5-415
Muñoz-Nava, L. M., Alvarez, H. A., Flores-Flores, M., Chara, O. and Nahmad, M. (2020). A dynamic cell recruitment process drives growth of the *Drosophila* wing by overscaling the vestigial expression pattern. *Dev. Biol* **462**, 141-151. doi:10.1016/j.ydbio.2020.03.009
Nel, A., Roques, P., Nel, P., Prokin, A. A., Bourgoin, T., Prokop, J., Szwedo, J., Azar, D., Desutter-Grandcolas, L., Wappler, T. et al. (2013). The earliest known holometabolous insects. *Nature* **503**, 257-261. doi:10.1038/nature12629
Neto-Silva, R. M., Wells, B. S., Johnston, L. A. (2009). Mechanisms of growth and homeostasis in the *Drosophila* wing. *Annu. Rev. Cell Dev. Biol* **25**, 197-220. doi:10.1146/annurev.cellbio.24.110707.175242
Neumann, C. J. and Cohen, S. M. (1996). A hierarchy of cross-regulation involving Notch, wingless, vestigial and cut organizes the dorsal/ventral axis of the *Drosophila* wing. *Development* **122**, 3477-3485. doi:10.1242/dev.122.11.3477
Okada, Y., Katsuki, M., Okamoto, N., Fujioka, H. and Okada, K. (2019). A specific type of insulin-like peptide regulates the conditional growth of a beetle weapon. *PLoS Biol.* **17**, e3000541. doi:10.1371/journal.pbio.3000541
Parker, J. and Struhl, G. (2020). Control of *Drosophila* wing size by morphogen range and hormonal gating. *Proc. Natl. Acad. Sci. U. S. A* **117**, 31935-31944. doi:10.1073/pnas.2018196117
Pélabon, C., Firmat, C., Bolstad, G. H., Voje, K. L., Houle, D., Cassara, J., Le Rouzic, A. and Hansen, T. F. (2014). Evolution of morphological allometry. *Ann. N. Y. Acad. Sci* **1320**, 58-75. doi:10.1111/nyas.12470
Port, F., Chen, H.-M., Lee, T. and Bullock, S. L. (2014). Optimized CRISPR/Cas tools for efficient germline and somatic genome engineering in *Drosophila*. *Proc. Natl. Acad. Sci. U. S. A* **111**, E2967-E2976. doi:10.1073/pnas.1405500111
Powell, J. R. and DeSalle, R. (1995). *Drosophila* molecular phylogenies and their uses. In *Evolutionary Biology* (ed. M. K. Hecht, R. J. Macintyre, M. T. Clegg), pp. 87-138. Boston, MA: Springer US.
Prasad, M., Bajpai, R. and Shashidhara, L. S. (2003). Regulation of Wingless and Vestigial expression in wing and haltere discs of *Drosophila*. *Development* **130**, 1537-1547. doi:10.1242/dev.00393
Prasad, N., Tarikere, S., Khanale, D., Habib, F. and Shashidhara, L. S. (2016). A comparative genomic analysis of targets of Hox protein Ultrabithorax amongst distant insect species. *Sci. Rep* **6**, 27885. doi:10.1038/srep27885
Rebeiz, M. and Tsiantis, M. (2017). Enhancer evolution and the origins of morphological novelty. *Curr. Opin. Genet. Dev* **45**, 115-123. doi:10.1016/j.gde.2017.04.006
Reigada, C. and Godoy, W. A. C. (2005). Seasonal fecundity and body size in *Chrysomya megacephala* (Fabricius) (Diptera: Calliphoridae). *Neotrop. Entomol* **34, 163-168**.
Rohner, P. T., Teder, T., Esperk, T., Lüpold, S. and Blanckenhorn, W. U. (2018). The evolution of male–biased sexual size dimorphism is associated with increased body size plasticity in males. *Funct. Ecol* **32**, 581-591. doi:10.1111/1365-2435.13004
Ryan, G. E. and Farley, E. K. (2020). Functional genomic approaches to elucidate the role of enhancers during development. *Wiley Interdiscip. Rev. Syst. Biol. Med* **12**, e1467.
Sagarra, L. A., Vincent, C. and Stewart, R. K. (2001). Body size as an indicator of parasitoid quality in male and female *Anagyrus kamali* (Hymenoptera: Encyrtidae). *Bull. Entomol. Res* **91**, 363-368. doi:10.1079/ber2001121
Schneider, C. A., Rasband, W. S. and Eliceiri, K. W. (2012). NIH Image to ImageJ: 25 years of image analysis. *Nat. Methods* **9**, 671-675. doi:10.1038/nmeth.2089
Schoofs, A., Niederegger, S., van Ooyen, A., Heinzel, H.-G. and Spiess, R. (2010). The brain can eat: establishing the existence of a central pattern generator for feeding in third instar larvae of *Drosophila virilis* and *Drosophila melanogaster*. *J. Insect Physiol* **56**, 695-705. doi:10.1016/j.jinsphys.2009.12.008
Shingleton, A. W. (2010). Allometry: the study of biological scaling. *Nat. Educ. Knowl.* 3:2.
Shingleton, A. W. (2019). Which line to follow? The utility of different line-fitting methods to capture the mechanism of morphological scaling. *Integr. Comp. Biol* **59**, 1399-1410.
Shingleton, A. W., Mirth, C. K. and Bates, P. W. (2008). Developmental model of static allometry in holometabolous insects. *Proc. R. Soc. B Biol. Sci* **275**, 1875-1885. doi:10.1098/rspb.2008.0227
Shingleton, A. W., Estep, C. M., Driscoll, M. V. and Dworkin, I. (2009). Many ways to be small: different environmental regulators of size generate distinct scaling relationships in *Drosophila melanogaster*. *Proceedings. Biol. Sci* **276**, 2625-2633.
Simmonds, A. J., Liu, X., Soanes, K. H., Krause, H. M., Irvine, K. D. and Bell, J. B. (1998). Molecular interactions between Vestigial and Scalloped promote wing formation in *Drosophila*. *Genes Dev.* **12**, 3815-3820. doi:10.1101/gad.12.24.3815
Simons, E. A. and Frost, S. R. (2021). Ontogenetic allometry and scaling in catarrhine crania. *J. Anat* **238**, 693-710. doi:10.1111/joa.13331
Smith, T. F. and Waterman, M. S. (1981). Identification of common molecular subsequences. *J. Mol. Biol* **147**, 195-197. doi:10.1016/0022-2836(81)90087-5
Stern, D. L. and Orgogozo, V. (2009). Is genetic evolution predictable? *Science* **323**, 746-751. doi:10.1126/science.1158997
Stillwell, R. C., Dworkin, I., Shingleton, A. W. and Frankino, W. A. (2011). Experimental manipulation of body size to estimate morphological scaling relationships in *Drosophila*. *J. Vis. Exp.* **56**, e3162. doi:10.3791/3162
Tang, H. Y., Smith-Caldas, M. S. B., Driscoll, M. V., Salhadar, S. and Shingleton, A. W. (2011). FOXO regulates organ-specific phenotypic plasticity in *Drosophila*. *PLoS Genet.* **7**, e1002373. doi:10.1371/journal.pgen.1002373

Thorne, A. D., Pexton, J. J., Dytham, C. and Mayhew, P. J. (2006). Small body size in an insect shifts development, prior to adult eclosion, towards early reproduction. *Proc. R. Soc. B Biol. Sci.* **273**, 1099-1103. doi:10.1098/rspb.2005.3416

Tidière, M., Lemaître, J.-F., Pélabon, C., Gimenez, O. and Gaillard, J.-M. (2017). Evolutionary allometry reveals a shift in selection pressure on male horn size. *J. Evol. Biol* **30**, 1826-1835. doi:10.1111/jeb.13142

Tran, A. K., Hutchison, W. D. and Asplen, M. K. (2020). Morphometric criteria to differentiate *Drosophila suzukii* (Diptera: Drosophilidae) seasonal morphs. *PLoS One* **15**, e0228780.

Tripathi, B. K. and Irvine, K. D. (2022). The wing imaginal disc. *Genetics* **220**, iyac020. doi:10.1093/genetics/iyac020

Uller, T., Moczek, A. P., Watson, R. A., Brakefield, P. M. and Laland, K. N. (2018). Developmental bias and evolution: a regulatory network perspective. *Genetics* **209**, 949-966. doi:10.1534/genetics.118.300995

Van Belleghem, S. M., Alicea Roman, P. A., Carbia Gutierrez, H., Counterman, B. A. and Papa, R. (2020). Perfect mimicry between *Heliconius* butterflies is constrained by genetics and development. *Proc. R. Soc. B Biol. Sci.* **287**, 20201267. doi:10.1098/rspb.2020.1267

Watson, J. F. and García-Nafría, J. (2019). *In vivo* DNA assembly using common laboratory bacteria: a re-emerging tool to simplify molecular cloning. *J. Biol. Chem* **294**, 15271-15281. doi:10.1074/jbc.REV119.009109

Warton, D. I., Wright, I. J., Falster, D. S. and Westoby, M. (2006). Bivariate line-fitting methods for allometry. *Biol. Rev. Camb. Philos. Soc* **81**, 259-291. doi:10.1017/S1464793106007007

Warton, D. I., Duursma, R. A., Falster, D. S. and Taskinen, S. (2012). smatr 3 – an R package for estimation and inference about allometric lines. *Methods Ecol. Evol* **3**, 257-259. doi:10.1111/j.2041-210X.2011.00153.x

Weber, K. E. (1990). Selection on wing allometry in *Drosophila melanogaster*. *Genetics* **126**, 975-989. doi:10.1093/genetics/126.4.975

Weiss, A., Charbonnier, E., Ellertsdóttir, E., Tsirigos, A., Wolf, C., Schuh, R., Pyrowolakis, G. and Affolter, M. (2010). A conserved activation element in BMP signaling during *Drosophila* development. *Nat. Struct. Mol. Biol* **17**, 69-76. doi:10.1038/nsmb.1715

Wilcox, A. S., Vea, I. M., Frankino, W. A. and Shingleton, A. W. (2023). Genetic variation of morphological scaling in *Drosophila melanogaster*. *Heredity* doi:10.1038/s41437-023-00603-y

Williams, J. A., Bell, J. B. and Carroll, S. B. (1991). Control of Drosophila wing and haltere development by the nuclear vestigial gene product. *Genes Dev.* **5**, 2481-2495. doi:10.1101/gad.5.12b.2481

Wittkopp, P. J. and Kalay, G. (2011). *Cis*-regulatory elements: molecular mechanisms and evolutionary processes underlying divergence. *Nat. Rev. Genet* **13**, 59-69. doi:10.1038/nrg3095

Wray, G. A. (2003). The evolution of transcriptional regulation in eukaryotes. *Mol. Biol. Evol* **20**, 1377-1419. doi:10.1093/molbev/msg140

Wray, G. A. (2007). The evolutionary significance of *cis*-regulatory mutations. *Nat. Rev. Genet* **8**, 206-216. doi:10.1038/nrg2063

Xu, H.-J., Xue, J., Lu, B., Zhang, X.-C., Zhuo, J.-C., He, S.-F., Ma, X.-F., Jiang, Y.-Q., Fan, H.-W., Xu, J.-Y. et al. (2015). Two insulin receptors determine alternative wing morphs in planthoppers. *Nature* **519**, 464-467. doi:10.1038/nature14286

Zecca, M. and Struhl, G. (2007a). Recruitment of cells into the *Drosophila* wing primordium by a feed-forward circuit of vestigial autoregulation. *Development* **134**, 3001-3010. doi:10.1242/dev.006411

Zecca, M. and Struhl, G. (2007b). Control of *Drosophila* wing growth by the vestigial quadrant enhancer. *Development* **134**, 3011-3020. doi:10.1242/dev.006445

Zecca, M. and Struhl, G. (2010). A feed-forward circuit linking wingless, fat-dachsous signaling, and the warts-hippo pathway to *Drosophila* wing growth. *PLoS Biol.* **8**, e1000386. doi:10.1371/journal.pbio.1000386

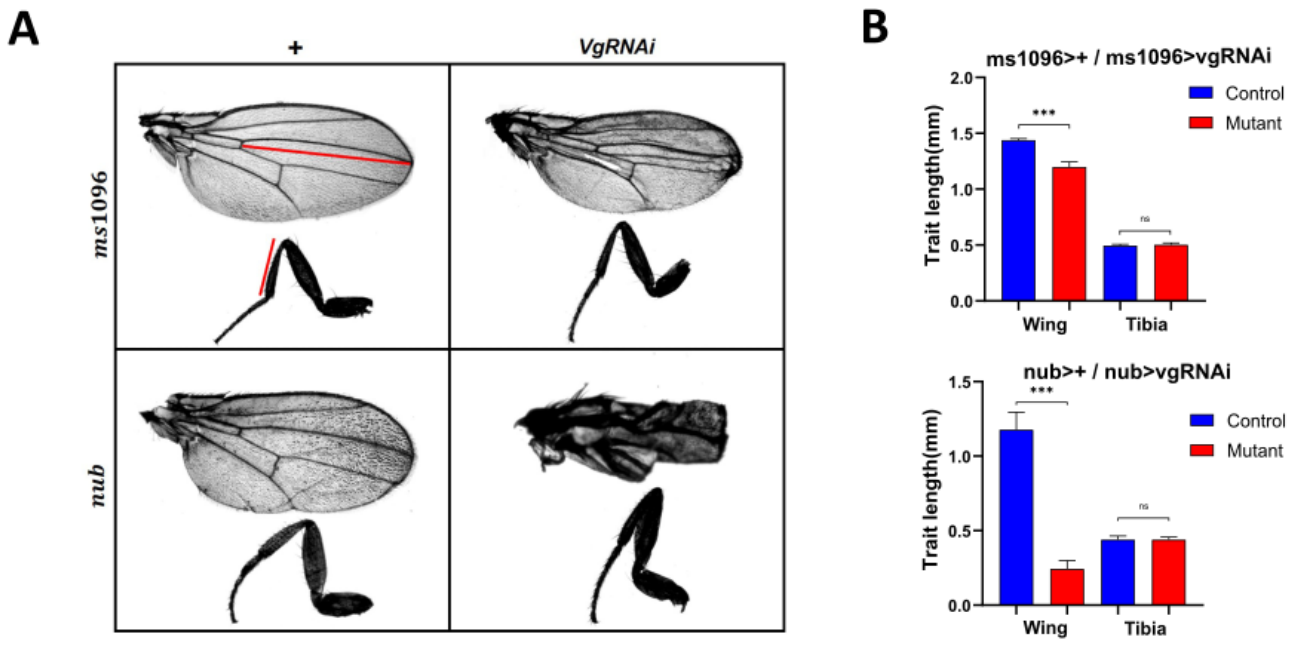

Fig. S1. Legs are not affected by changes in *vg* expression (A) Wing and tibia phenotypes of *D. melanogaster* flies expressing a vgRNAi under the control of ms1096Gal4 or nubGal4 compared to the corresponding controls (ms1096>+ or nub>+, respectively). P/D lengths in wings and tibias were taken to determine wing/tibia scaling relationships in Fig. 2, S2, 4, S4 (red lines). (B) Quantification of tibia and wing P/D lengths of the genotypes shown in A. Mutants (red bars) correspond to the vgRNAi-expressing flies. Statistical comparisons correspond to Student t-tests. ***=*p-value<0.001, ns* = not statistically significant (*p-value>0.05*). ms1096>vgRNAi, *n*= 13; ms1096>+, *n*= 10; nub>vgRNAi, *n*= 9; nub>+, *n*= 7.

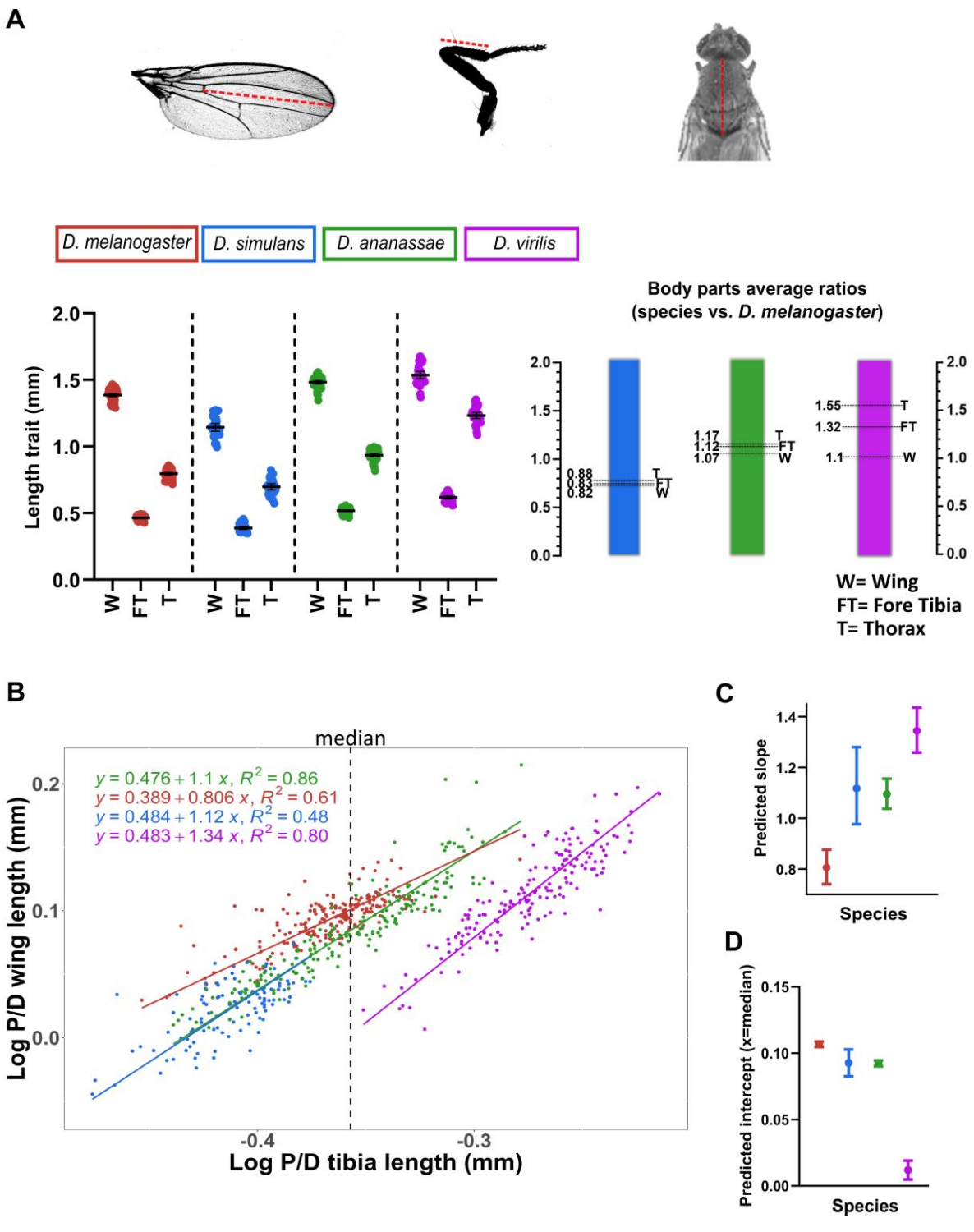

Fig. S2. Wing-to-tibia scaling relationships reveal a reduction of wing size in *D. virilis* males. (A) P/D trait measures in *Drosophila* species. Average length of left/right wings and fore tibias, as well as thorax measures are represented for each male flies. Right panel shows the body parts average ratios (species vs. *D. melanogaster*) for each measured trait. *D. melanogaster n*= 60, *D. simulans n*=30, *D. ananassae n*=58, *D. virilis n*=34. (B) Wing-to-tibia static scaling relationships fitted using model II of regression (SMA) in male *Drosophila*. Red, blue, green and purple dots correspond to *D. melanogaster, D. simulans, D. ananassae* and *D. virilis* respectively. (C) Predicted slope of wing-tibia scaling relationship for each *Drosophila* species. (D) Predicted intercept of wing-tibia scaling relationship for each *Drosophila* species. The predicted intercept value was obtained through SMA adjusted to the median log(tibia) of all species (dotted line in panel B). Error bars are 95% confidence intervals. The experiment was replicated two times in the laboratory. *D. melanogaster, n*=215; *D. simulans, n*=112; *D. ananassae, n*=195; *D. virilis, n*=179. T=thorax; FT=fore tibia; W=wing.

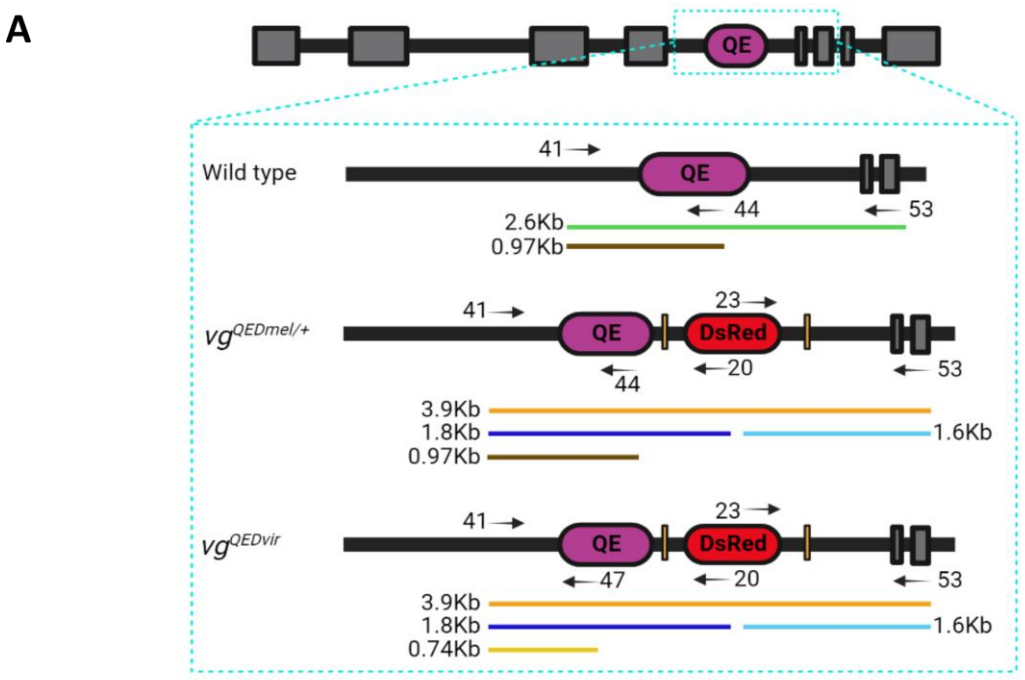

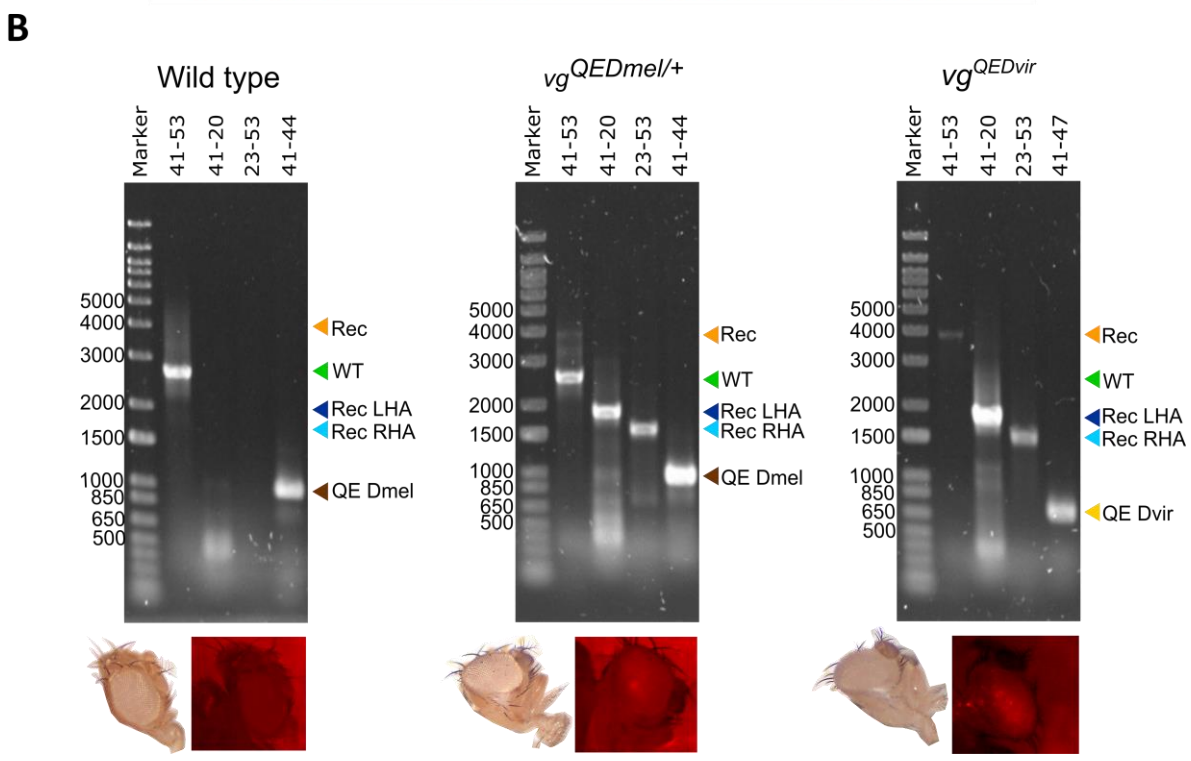

Fig. S3. Molecular confirmation of the *vg*^{QE} replacement. (A) Size of amplification products used for the identification of the *vg*^{QE} replacement are shown in the colored lines. Primers and the sense that were used are indicated with black arrows. (B) Amplification products in wild type, *vg*^{QEDmel}/+, and *vg*^{QEDvir}/*vg*^{QEDvir} flies. We used oligos 41 and 53 (see Table S1) for the evaluation of the Recombinant (Rec) and/or the wild-type (WT) product; oligos 41 and 20 (see Table S1) were used for the identification of the Recombinant Left homologous Arm (Rec-LHA); oligos 23 and 53 (see Table S1) were used for the amplification of the Recombinant Right Homologous Arm (RecRHA); *vg*^{QEDmel}/+, and *vg*^{QEDvir}/*vg*^{QEDvir} were evaluated with oligos 41 and, 44 or 47 (see Table S1), respectively. At the bottom panels, evidence of fluorescent eyes is shown as a confirmation that the DsRed marker is present.

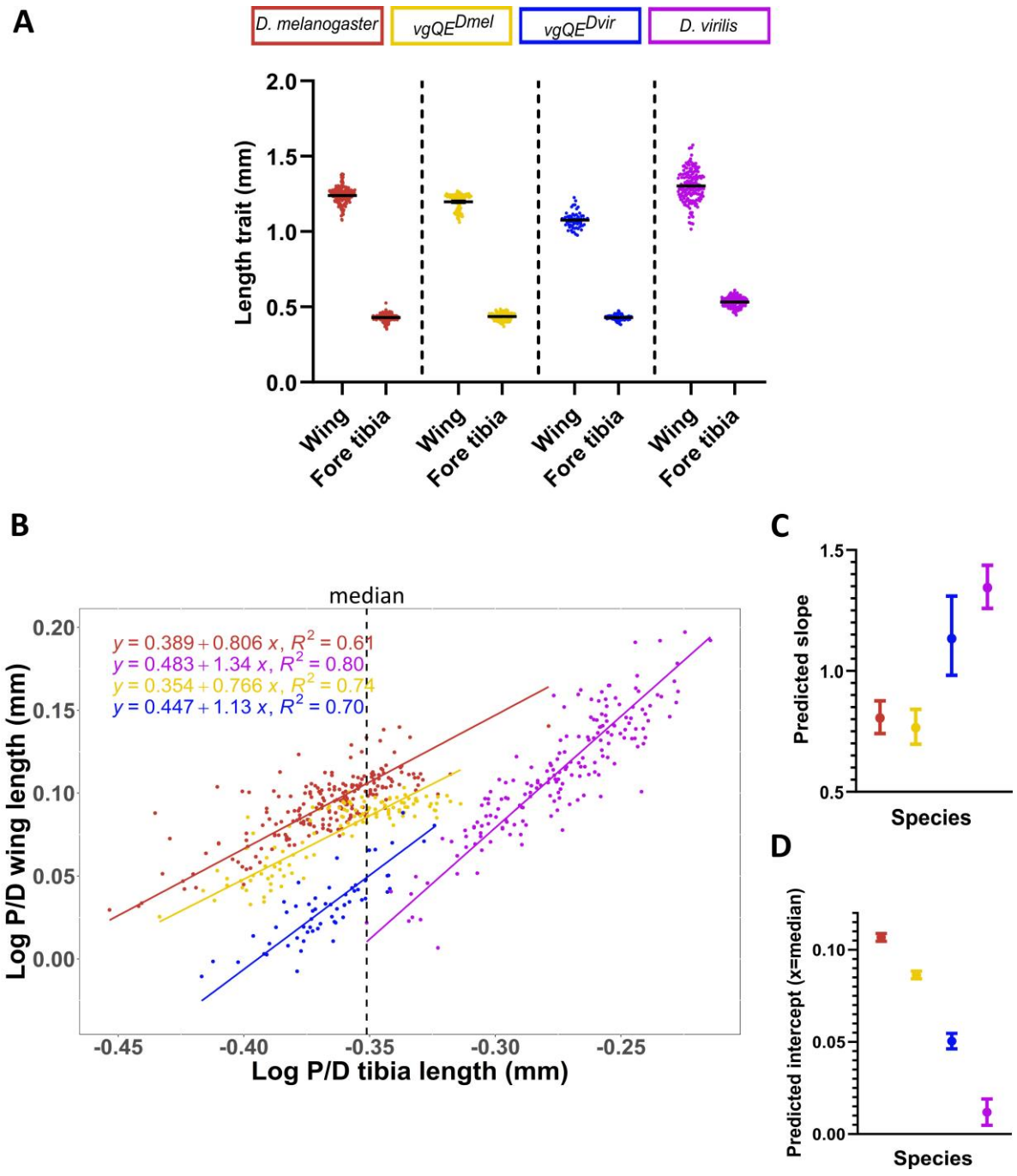

Fig. S4. *D. virilis vg*^{QE} replacement into *D. melanogaster* results in allometric changes in males. (A) Proximal-distal trait measures in *Drosophila* species (*D. melanogaster, D.virilis)* and CRISPR/Cas9 mutants (*vg*^{QEDmel}, *vg*^{QEDvir}). Average length of left/right wings and fore tibias are represented for each male flies. (B) Wing-to-tibia static static relationships fitted using model II of regression (SMA).

Yellow and blue lines and dots correspond to HDR replacements using *vg*^{QEDmel} and *vg*^{QEDvir} respectively. Red and purple lines and dots show the scaling relationship in *D. melanogaster* and *D. virilis* wild type animals respectively. (C) Predicted slope of wing-tibia scaling relationship for *D. melanogaster, D. virilis,* and the CRISPR/Cas9 edited stocks. (D) Predicted intercept of wing-tibia scaling relationship for *D. melanogaster, D. virilis,* and the CRISPR/Cas9 edited stocks. The predicted intercept value was obtained through SMA adjusted to the overall median log(tibia size) of *D. melanogaster*, *D. virilis* and CRISPR/Cas9 stocks (dotted line in panel B). Error bars are 95% confidence intervals. *D. melanogaster, n*= 215; *vg*^{QEDmel}, *n*=118; *vg*^{QEDvir}, *n*=59' *D. virilis, n*=179.

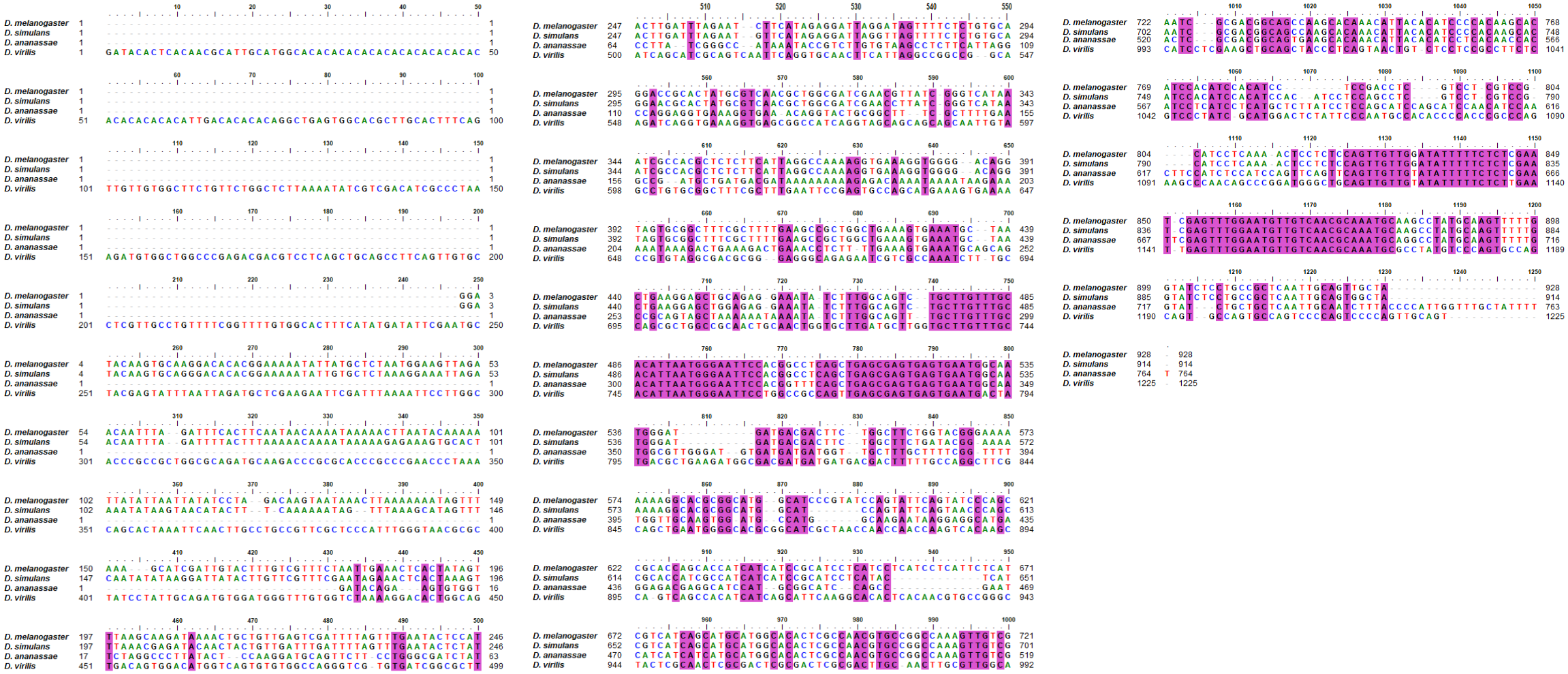

Fig. S5. Multiple alignment of QE sequences in *Drosophila* species. Sequences obtained from local alignments using the Smith–Waterman algorithm were processed in Clustal Omega for multiple alignment. Conserved bases in the four species are highlighted in pink.

Table S1. Oligonucleotides

N°	Oligo name	Sequence
2	QE3’	GCTATTTCTAGCTCTAAAACTTATGTGTAATGGAGCTCCCGACGTTAAATTGAAAATAGGTC
3	TEA2	GGAAAGATATCCGGGTGAACTTCGCAGTATGGTGATTCGATTCGTTTTAGAGCTAGAAATAGCAAG
20	mCherry-R	CTTGGTCACCTTCAGCTTGG
23	DsRed1C Forward	GGACATCACCTCCCACAACG
41	RecDsp F	GCCGCATAGATTCCTCATTACG
44	QE sp R	CATTCACTCACTCGCTCAGCTG
47	QE vir R	GATTTGGCGACGATTCTCTGC
53	Outside_screening_R	CGATCGGGCGATCGACTCAC
352	M13 Forward	TGTAAAACGACGGCCAGT
596	pCFD4 upstream seq	TAGTCCCATCATTGGCATGGTAGGTACCCG
835	pBR322 fwd	CAGCTCGAGGCTCTTCCGTCAATCG
836	pBR322 rev	CTAGCATGCAAGAATTCCACCTGC
837	DsRed fwd	CGGCCGCGGACATATGCACACCTG
838	DsRed rev	TGGAGATCTTTACTAGTGCTCTTC
839	DmLHA2/pBR322 fwd	GTGGAATTCTTGCATGCTAGGCCACTCGCTTGTTCTTTCGATTTC
840	DmLHA2/DsRed rev	TGTGCATATGTCCGCGGCCGTCGAATCACCATACTGCATTTGGTG
841	DmRHA1/DsRed fwd	AGCACTAGTAAAGATCTCCATAATGGAGATGTCTTGCTCCCGGC
842	DmRHA1/pBR322 rev	GACGGAAGAGCCTCGAGCTGCCTACAAGCAGATATCCGATTGG
843	DmLHA2 rev	TCGAATCACCATACTGCATTTGGTG
844	Dmel/virQE fwd	AATGCAGTATGGTGATTCGACTAGTTGGAATGTGCTAT
845	DmelQE rev	TGTGCATATGTCCGCGGCCGTGTGTAATGGAGCTCCC
846	DvirQE rev	TGTGCATATGTCCGCGGCCGAGTGTAATGGAGCTCTG